NASA TN D-962

TECHNICAL NOTE

D-962

LAMINAR HEAT-TRANSFER AND PRESSURE MEASUREMENTS AT A MACH NUMBER OF 6 ON SHARP AND BLUNT 15° HALF-ANGLE CONES AT ANGLES OF ATTACK UP TO 90°

By Raul J. Conti

Langley Research Center
Langley Air Force Base, Va.

NATIONAL AERONAUTICS AND SPACE ADMINISTRATION
WASHINGTON

October 1961

NATIONAL AERONAUTICS AND SPACE ADMINISTRATION

TECHNICAL NOTE D-962

LAMINAR HEAT-TRANSFER AND PRESSURE MEASUREMENTS AT A MACH NUMBER OF 6 ON SHARP AND BLUNT 15° HALF-ANGLE CONES AT ANGLES OF ATTACK UP TO 90°

By Raul J. Conti

SUMMARY

Two circular conical configurations having 15° half-angles were tested in laminar boundary layer at a Mach number of 6 and angles of attack up to 90°. One cone had a sharp nose and a fineness ratio of 1.87 and the other had a spherically blunted nose with a bluntness ratio of 0.1428 and a fineness ratio of 1.66. Pressure measurements and schlieren pictures of the flow showed that near-conical flow existed up to an angle of attack of approximately 60°. At angles of attack above 70° high-pressure areas were present near the base and the bow shock wave was considerably curved.

Comparison of the results with simply applied theories showed that on the stagnation line pressures may be predicted by Newtonian theory, and heat transfer by local yawed-cylinder theory based on the yaw angle of the windward generator and the local radius of the cone. Base effects increased the heat transfer in a region extending forward approximately 15 to 30 percent of the windward generator. Circumferential pressure distributions were higher than the corresponding Newtonian distribution and a better prediction was obtained by modifying the theory to match the pressure at 90° from the windward generator to that on the surface of the cone at an angle of attack of 0°. Circumferential heat-transfer distributions were predicted satisfactorily up to about 60° from the stagnation line by using Lees' heat-flux distribution based on the Newtonian pressure. The effects of nose bluntness at large angles of attack were very small in the region beyond two nose radii from the point of tangency.

INTRODUCTION

The circular cone is a basic aerodynamic shape and as such it has been the subject of numerous investigations. Sharp and blunt cones in both laminar and turbulent flows have been studied at zero and small

angles of attack. (See refs. 1 to 4.) However, the range of high angles of attack (30° to 90°) has not yet been as extensively investigated. At these very large angles the flow on finite cones may be expected to depart from the conical or near-conical flow characteristic of the smaller angles of attack. Moreover, the effect of the finite length of the cone may become more predominant at higher angles, thus introducing a scale effect that would further complicate the picture.

At the present time reentry configurations that make use of the circular cone as a basic shape are under consideration; therefore, the possibility of heating problems at very large angles of attack must be considered. This possibility prompted the present investigation, wherein two particular conical shapes in laminar flow were studied at angles of attack up to 90°. The principal aim of this investigation was to determine whether a simple method of predicting pressure distributions and heating rates may be applied to this problem. To this end, the experimental data obtained are compared to the values predicted by local yawed-cylinder and Newtonian theories.

L 1624

SYMBOLS

c specific heat of skin material

C_p pressure coefficient, $\frac{p - p_\infty}{q_\infty}$

$C_{p,max}$ maximum pressure coefficient, $\frac{p_{t,2} - p_\infty}{q_\infty}$

C_p^* modified pressure coefficient, $\frac{p - p_c}{q_\infty}$

C_Y heat-conduction parameter from reference 6, $\frac{1}{k_b} \frac{R^2}{l\left(1 - \frac{1}{2}\frac{l}{R}\right)} h_s$

h heat-transfer coefficient corrected for conduction, $\frac{\dot{q}_w}{T_{aw} - T_w}$

h_i indicated heat-transfer coefficient, defined by equation (1)

k_b thermal conductivity of skin material

l	skin thickness
l_{eff}	effective skin thickness, $l\left(1 - \frac{1}{2}\frac{l}{x' \tan \phi}\right)$
M	Mach number
p	pressure
q	dynamic pressure
$\dot{q}$	heat flow per unit time and area
R	local radius of cone
Re	Reynolds number per foot
T	temperature
t	time
V	velocity
x'	distance measured along cone element from apex (or virtual apex) of cone
α	angle of attack
γ	ratio of specific heats for air, 7/5
η_r	recovery factor, $\frac{T_{aw} - T_e}{T_t - T_e}$
θ	circumferential angle measured about axis of cone from windward generator
Λ	yaw angle of windward generator
ρ	density of skin material
ϕ	cone half-angle

Subscripts:

aw	adiabatic wall
c	conditions on the surface of the cone at an angle of attack of 0^o

s	conditions on stagnation line of yawed cone (windward generator)
w	wall
t	isentropic stagnation conditions
∞	free-stream conditions
2	conditions behind normal shock
e	local conditions external to boundary layer

TEST FACILITY

The present tests were conducted in the Mach number 6.2 blowdown tunnel at the Langley Reentry Physics laboratory which has an enclosed test area of 12 by 14 inches in cross section. Transient heat-transfer testing utilizes a model injection mechanism which permits rapid injection of the model into the steady airstream. A detailed description of the facility is included in reference 5. The present tests were conducted at stagnation pressures of approximately 90 and 360 lb/sq in. abs and at stagnation temperatures of approximately 425° F and 475° F, respectively, yielding free-stream Reynolds numbers per foot of 1.53×10^6 and 6×10^6. Under these conditions the Mach number in the test area is 6.1 ± 0.07.

MODELS AND INSTRUMENTATION

Two models were tested: a 15° half-angle sharp cone and a 15° half-angle spherically blunted cone having fineness ratios of 1.87 and 1.66, respectively, and a bluntness ratio (ratio of nose radius to base radius) of 0.1428 for the blunt cone. (See fig. 1.) Both models were made from 22 gage type 347 stainless-steel sheet. The finished blunt cone had a wall thickness of 0.030 ± 0.001 inch, but the sharp cone had an appreciable longitudinal thickness variation which was measured after the tests were completed and is shown in figure 1. The models were mounted on a strut with an adapter that permitted roll angles about the cone axis up to 360° and angles of attack up to 90°. The strut was in turn mounted on the pneumatic injection mechanism on the top wall of the tunnel. Figure 2 shows the blunt cone mounted on the strut.

Instrumentation consisted of two rows of chromel-alumel thermocouples spot-welded to the inside surface of the cones along two generators 90° apart, as shown in figure 1. One row of pressure orifices having 0.040-inch inside diameters was located in each cone along a generator opposite one of the thermocouple rows. The angular location of thermocouples or pressure orifices about the axis of the cone is given by the angle θ, measured in either side of the sagittal plane of the cone from 0° to 90°, 0° corresponding to the forward stagnation line, otherwise denoted as windward generator. At an angle of attack of 0° the previous convention is extended so that $\theta = 0°$ corresponds to the upper generator (towards the top wall of the tunnel).

DATA RECORDING

The output of the thermocouples was fed into a Beckman 210 high-speed analog to digital data recording system. This is a high-impedance system that samples the output voltage of each thermocouple at a rate of 40 times per second, converts it to a binary digital system, and records it on magnetic tape. For the present tests the sensitivity of this system was 400 counts per millivolt which corresponds to 0.11° F per count. The background noise of the system is approximately ±3 counts; therefore, the thermocouple output was recorded within $\pm\frac{1}{3}$° F. Also recorded by the Beckman 210 were the stagnation temperature and pressure, the test-section static pressure, and the output of a circuit including two microswitches that showed the times at which the model injection started and was completed, respectively. The outputs of six preselected thermocouples, one tunnel static-pressure transducer, and the model injection marker were monitored by means of a Sanborn model 150 recorder.

Pressures were measured by means of a mercury manometer board. From photographs of the manometer board the pressure was read within ±0.03 inch of mercury, which corresponds to a maximum error in $p/p_{t,\infty}$ of about 2 percent.

Two photographs of the flow about the model were taken during each run by means of a single-path schlieren system with a light source having an effective flash duration of 4 microseconds. A horizontal wire was stretched across the tunnel windows to indicate the tunnel center line.

DATA REDUCTION

General

The pressure measurements were made under steady-state conditions. A series of photographs of the manometer board were taken during each run and pressures were recorded after two successive photographs showed the same readings.

The heat-transfer measurements were made during transient heating of the model. The tunnel was started with the model out of the test section, and after the static and stagnation pressures attained steady values, the model was injected into the airstream. During the subsequent heating of the model, the skin-temperature history was recorded as described previously.

Prior to injection the model was at constant room temperature. The injection process was completed in 0.25 second of which approximately only the last 0.05 second corresponded to actual travel in the airstream. Since the injection mechanism is enclosed in a box kept at tunnel static pressure, the injection process did not significantly influence the flow ahead of the test section. Consequently, in this way the initially isothermal model was subjected to nearly a step function in the driving potential for heat transfer $T_{aw} - T_w$. Under these conditions the heat-transfer coefficient was computed by means of the following equation:

$$h_i = \rho c l_{eff} \frac{\partial T_w / \partial t}{T_{aw} - T_w} \tag{1}$$

The effective skin thickness $l_{eff} = l\left(1 - \frac{1}{2}\frac{l}{x' \tan \phi}\right)$ is the volume per unit exposed area of a skin element at a distance x' from the cone apex. (See ref. 6.)

The adiabatic wall temperature T_{aw} was calculated by means of

$$\frac{T_{aw}}{T_e} = 1 + \eta_r \frac{\gamma - 1}{2} M_e^2$$

where a recovery factor $\eta_r = 0.84$ was used, and the Mach number was computed on the basis of the measured pressures on the surface of the

cone and the entropy level corresponding to the measured bow shock-wave inclination. For $\alpha > 60^\circ$ the sagittal cross section of the shock wave departed progressively from a straight line. The entropy level was determined for $\alpha = 70^\circ$ and $\alpha = 80^\circ$ by using average shock inclinations, whereas for $\alpha = 90^\circ$ normal-shock entropy was used. It was estimated that the errors introduced by these approximations are not significant. For instance, at $\alpha = 90^\circ$ and under the conditions of the present tests the difference in entropy level corresponding to the maximum inclination of the shock (about 26°) and that corresponding to the normal shock results in a maximum difference in h_i of less than 5 percent.

The slope $\partial T_w/\partial t$ was computed from the temperature history of each thermocouple by means of an IBM type 650 computer system. This computer was programed to fit the data recorded by the Bechman 210 system with a least-squares curve of the second degree in t. Two independent curves were fitted to the data, each curve covering a time interval of 0.5 second (20 data points) and in such a way that the last point of the first curve coincided with the first point of the second curve, to cover a total time interval of 1 second. The first curve fit was started about 0.3 second after the temperature started to rise ($t = 0$) at which time it was estimated that the initial errors introduced by heat conduction across the skin and disturbances associated with the injection process were small enough to be neglected. Further details of the curve-fitting and evaluation processes are included in reference 5. From the two curves thus fitted to the data the slope was computed at 0.100, 0.225, 0.350, 0.575, 0.700, and 0.825 second after the first point of the first curve. The appropriate constants and temperatures required to compute h_i from equation (1) were included in the program so that the IBM 650 printed six values of h_i (at the six times previously mentioned) for each thermocouple.

Heat-Conduction Corrections

Equation (1) does not take into consideration the effects of heat conduction in the skin of the model. In the present case of conical shapes tested through a wide range of angles of attack the heat-conduction problem becomes complicated since significant heat conduction may occur in more than one direction, and at the large angles of attack the conical shape implies a "change of scale" along x' in the heat-conduction problem. In this investigation, model design and testing techniques were chosen so as to keep heat conduction in the x' direction small enough to be neglected with respect to the aerodynamic heat input. However, at large angles of attack, circumferential heat conduction becomes significant. As mentioned before, for these models there is a change in scale as the local radius of the cone changes. Consequently, for a given testing time sections near the tip of the cone sustain

larger circumferential conduction errors than those far from the tip. These heat-conduction effects were evidenced in the present tests by consistent increases or decreases with time of the six successive values of h_i discussed in the previous section.

On the stagnation line h_i showed an approximately linear decrease with time (i.e., a net loss of heat due to conduction) and corrected values of the heat-transfer coefficient h were obtained by the method of reference 6. The results presented in that reference for h_i/h at the stagnation line of a cylindrical shell for several values of the heat-conduction parameter C_Y were used locally for each station on the cone having the same radius as that of the cylindrical shell. The parameter C_Y was calculated with the use of values of h_i. This local treatment of the problem appeared to be satisfactory since it yielded values of h that were constant in time within a few percent. The largest correction made was approximately 11 percent of the measured value at $x' = 1$ inch. At $x' > 2$ inches conduction errors were not significant and no corrections were made. For the circumferential h_i distribution ($\theta > 0^\circ$) only the data having negligible conduction ($x' \geqq 1.5$ inch) are presented.

L 1624

THEORIES USED FOR COMPARISON WITH DATA

Pressure Distributions

On the stagnation line two values of C_p were theoretically computed for each angle of attack by means of (a) modified Newtonian theory, and (b) pressure on the stagnation line of a yawed cylinder. The modified Newtonian pressure coefficient was computed from

$$C_{p,s} = C_{p,max} \cos^2\Lambda \tag{2}$$

where $C_{p,max}$ is the pressure coefficient corresponding to the stagnation region behind a normal shock wave at $M_\infty = 6.1$ and Λ is the yaw angle of the windward generator. The yawed-cylinder pressure coefficient was calculated from the following pressure ratio:

$$\frac{p_s}{p_{t,\infty}} = \frac{\left(\frac{\gamma+1}{2} M_\infty^2 \cos^2\Lambda\right)^{\frac{\gamma}{\gamma-1}} \left[\frac{\gamma+1}{2\gamma M_\infty^2 \cos^2\Lambda - (\gamma-1)}\right]^{\frac{1}{\gamma-1}}}{\left(1 + \frac{\gamma-1}{2} M_\infty^2\right)^{\frac{\gamma}{\gamma-1}}} \tag{3}$$

The circumferential pressure distribution p/p_s at a given angle of attack was obtained from the following modified Newtonian theories applied to the normal flow ($V_\infty \cos \Lambda$):

$$C_p = C_{p,s} \cos^2\theta \tag{4}$$

$$C_p^* = C_{p,s}^* \cos^2\theta \tag{5}$$

Equation (5) is an empirical modification where

$$C_p^* = \frac{p - p_c}{q_\infty}; \quad C_{p,s}^* = \frac{p_s - p_c}{q_\infty}$$

and p_c is the pressure on the surface of the cone at an angle of attack of 0° obtained from axisymmetric conical-flow theory.

Heat-Transfer Distributions

On the stagnation line the yawed-cylinder theory of reference 7 was used with the local radius of the cone and the flow component perpendicular to the windward generator. The velocity gradient was obtained from Newtonian theory. No effort was made to take into account the angularity between the shock wave and the windward generator of the cone. Computations were based on the following conditions:

$$M_\infty = 6.1; \quad T_t = 400^\circ \text{ F}; \quad T_w = 100^\circ \text{ F}$$

Circumferential heat-transfer distributions $h/h_s(\theta)$ were obtained from Lees' heat-flux distribution $\dot{q}_w/\dot{q}_{w,s}$ (ref. 8) applied to the normal-flow component on the basis of Newtonian pressures (eq. (4)). Adiabatic wall temperatures were computed by assuming an isentropic expansion from stagnation-line conditions to the local pressures given by equation (4) and by using a recovery factor η_r of 0.84. Stagnation-line pressures for these computations were calculated at each angle of attack by means of equation (3), and temperatures external to the boundary layer at the stagnation line were computed from the following equation:

$$\frac{T_s}{T_{t,\infty}} = \frac{1 + \frac{\gamma - 1}{2} M_\infty^2 \cos^2\Lambda}{1 + \frac{\gamma - 1}{2} M_\infty^2} \tag{6}$$

For the particular case of an angle of attack of 0° the results of reference 9 for flat-plate laminar flow were used together with Mangler's transformation in order to apply them to the present case.

DISCUSSION OF RESULTS

General

Heat-transfer and pressure measurements on the stagnation line are presented in figure 3 at angles of attack of 45°, 60°, 70°, 80°, and 90° and in figure 4 for an angle of attack of 0°. Pressure measurements on the stagnation line are also presented as a function of angle of attack in figure 5. Circumferential pressure distributions are shown in figure 6 and circumferential heat-transfer distributions are shown in figure 7. Figure 8 shows schlieren pictures of the flow about the models.

The good agreement of heat-transfer data with laminar theory at an angle of attack of 0° and the fact that at all angles of attack the data correlate within the experimental accuracy on the basis of $\sqrt{Re_\infty}$ are indications that the boundary layer was laminar for all of the present tests.

Free-stream disturbances were present upstream of the model as may be seen in the schlieren pictures. (See, for example, fig. 8(i).) The flow deflection across these disturbances was measured by means of a wedge and found to have a maximum of approximately $3/4^\circ$. Throughout the range of angles of attack of the models, the disturbances interfered with the bow shock resulting in corresponding perturbations in pressures and heat transfer. This effect was more noticeable on heat transfer at $\alpha = 70^\circ$ and $\alpha = 80^\circ$ at large Reynolds numbers where the disturbances can be expected to have a larger effect on the relatively low stagnation-line velocities.

A brief investigation of strut interference and scale effects due to base interference was made by schlieren observations. Two models geometrically similar to the sharp heat-transfer model, one being a full-scale version and the other a 0.68-scale version of the heat-transfer model, were sting-mounted to minimize strut interference and tested at $\alpha = 90^\circ$. Schlieren pictures of the flow pattern are shown in figure 8(k) for the full-scale model and 8(l) for the 0.68-scale model. Comparison of these pictures with figure 8(i) showing the heat-transfer model failed to show differences attributable to scale effects or strut interference.

Pressure Distributions

In figure 5 experimental values of $C_{p,s}/C_{p,max}$ are plotted against angle of attack and compared with Newtonian theory from equation (2). The experimental data agree with theory for $0^\circ < \alpha < 60^\circ$. At $\alpha > 60^\circ$ the experimental values are consistently smaller than theory, which is to be expected since Newtonian theory was applied disregarding the bow-shock inclination. In the present case the theory predicts $C_{p,s} = C_{p,max}$ at $\alpha = 75^\circ$, a condition that would exist if both the windward generator and the shock wave were normal to the free stream at this angle. However, this is not the case since at $\alpha = 75^\circ$ (where the windward generator is normal to the free stream) the bow shock is inclined. In the neighborhood of 70°, where the shock becomes normal (see fig. 8(g)), the windward generator is inclined and therefore has finite velocity. As a consequence, the experimental values of $C_{p,s}$ are always less than $C_{p,max}$, the maximum measured value of $C_{p,s}/C_{p,max}$ being 0.95. The effect of the different inclinations of the shock wave and the windward generator is present at all angles of attack but figure 5 shows that it becomes significant only at $\alpha > 60^\circ$.

L
1
6
2
4

Stagnation-line pressure distributions at several angles of attack are shown in figure 3 in the form of pressure coefficients $C_{p,s}$. It may be seen that at $\alpha = 45^\circ$ and $\alpha = 60^\circ$ the pressures do not appear to vary drastically along the cone element thus indicating flow with conical characteristics. At $\alpha = 70^\circ$ the picture is confused by the free-stream disturbances. At $\alpha = 80^\circ$ and $\alpha = 90^\circ$ there is a definite trend to depart from conical flow, with a maximum variation in $C_{p,s}$ of about 14 percent, which is attributed to the presence of stagnation points near the base of the cone behind the normal portion of the bow shock. These stagnation points were detected by visual observation of the oil flow patterns. At these two angles the pressure increase in the neighborhood of the tip was due to a free-stream disturbance. Results for the blunt cone are available at $\alpha = 45^\circ$, $\alpha = 60^\circ$, and $\alpha = 90^\circ$. No consistent significant differences with the sharp cone were observed, except at $x' = 2$ inches and $x' = 6$ inches at $\alpha = 90^\circ$.

The ratio of the experimental pressure at a given θ to the experimental pressure on the windward generator at the same value of x' is shown in figure 6 for various angles of attack. There is a general tendency for p/p_s to decrease along generators but deviations are not large; thus, it may be concluded that the pressure distribution along any generator on the windward side of the cone is essentially similar to that on the stagnation line. Normal-flow Newtonian pressures from equation (4) fall below the data, diverging progressively from the measurements as θ increases. Newtonian theory based on the

total free-stream velocity (not shown) still falls short of the measured pressures. The empirical modification of equation (5) is in better agreement with the data, especially at large values of θ. No significant differences were found between blunt- and sharp-cone pressure distributions.

At an angle of attack of 0° (see fig. 4) the pressure coefficient on the sharp cone is in good agreement with conical-flow theory. On the blunt cone the pressure coefficient is lower at $x' < 3$ inches and essentially the same as for the sharp cone at $x' > 3$ inches.

Heat-Transfer Distributions

Heat-transfer distributions on the stagnation line are presented in figure 3. Reasonable agreement between experimental data and local yawed-cylinder theory was found, and heat-transfer prediction by this method is believed to be appropriate at least for engineering computations. As mentioned before, at $\alpha = 70^\circ$ and $\alpha = 80^\circ$ when the windward generator is nearly perpendicular to the free stream a maximum effect of the free-stream disturbances discussed previously may be expected. This is evidenced in figures 3(c) and 3(d) by the data points at $x' = 2.5$ inches which have large scatter compared to the scatter at adjacent stations and to the scatter at the same station at lower and higher angles of attack. This may also be the explanation for the relatively high heat transfer at $\alpha = 70^\circ$ for $x' > 2.5$ inches. The increase in heat transfer near the base of the cone is attributed to base interference effects that would tend to increase the velocity gradient, and therefore the heat transfer, on the stagnation line. This base effect extended toward the apex approximately 15 percent of the windward generator length at $\alpha = 45^\circ$ and $\alpha = 60^\circ$, and approximately 30 percent at $\alpha = 80^\circ$ and $\alpha = 90^\circ$. Within the present experimental accuracy no significant difference was found between the blunt and sharp cones.

At an angle of attack of 0° (fig. 4) the heat-transfer data agree well with cone theory. The experimental heat-transfer coefficient for the blunt cone, which was computed on the basis of normal-shock entropy, is lower than that on the sharp cone at $x' < 3$ inches, which is consistent with the pressure distribution. The increase in heat transfer near the base of the sharp cone at the higher Reynolds number was due to strut interference in a narrow area near $\theta = 0^\circ$. This interference region appears as a white area along the top generator in the schlieren of figure 8(a).

Circumferential heat-transfer distributions are presented in figure 7 for stations at $x' \geq 1.5$ inches where heat-conduction effects

were negligible. The normalizing h_s used is an average (including both Reynolds numbers) of the experimental data on the windward generator of the particular sharp or blunt configuration being evaluated. As in the case of pressure distributions there appears to be a tendency of decreasing h/h_s with x'. Lees' heat-transfer distribution based on the Newtonian pressure of equation (4) predicts satisfactorily the heat-transfer distribution up to values of θ of about 60°. At $\theta > 60^\circ$ the theory is in general low at the angles of attack tested, and it is expected that a better prediction may be obtained by basing the heat-transfer distributions on the pressures given by equation (5). This task was not undertaken in the present investigation since the regions of main interest (because of high heating rates) were those nearer the stagnation line.

CONCLUDING REMARKS

In the course of this investigation two conical shapes consisting of sharp and blunt 15° half-angle cones were tested in laminar boundary-layer flow at a free-stream Mach number of 6.1 and angles of attack up to 90°. Free-stream disturbances originating upstream of the model with associated flow deflections up to a maximum of about $3/4^\circ$ resulted in perturbations in heat transfer and pressures on the cone, especially at an angle of attack of 70° where the perturbation had a relatively large effect on the low stagnation-line velocities. A brief attempt was made to determine qualitatively whether scale effects or strut interference existed at an angle of attack of 90°. For this purpose the flow patterns about a full-scale and a 0.68-scale sting-mounted model were observed and compared with the sharp-nose heat-transfer model. No indications of important strut interference or scale effects were found.

Stagnation Line

For angles of attack up to 60° the flow was nearly conical and the pressure coefficient was satisfactorily predicted by Newtonian theory. At larger angles of attack the experimental pressure coefficient was less than that predicted by Newtonian theory and variations of the pressure coefficient along the windward generator of up to 14 percent indicated a definite departure from conical flow which was substantiated by schlieren pictures of the bow shock wave.

Heat transfer at two free-stream Reynolds numbers was correlated on the basis of the square root of the Reynolds number per unit length and can be predicted for engineering computations at angles of attack up to 90° by means of local yawed-cylinder theory based on the yaw

angle of the windward generator and the local radius of the cone. A base effect which increased the heat-transfer coefficient in a region covering approximately 15 to 30 percent of the windward generator was observed at the angles of attack of this investigation.

Circumferential Distributions

Experimental pressure distributions were consistently higher than the values predicted by Newtonian theory. It was found that the pressures could be predicted more accurately by introducing a modification in the Newtonian theory that consists essentially in matching the pressure at 90° from the stagnation line with the pressure on the cone at an angle of attack of 0° for all angles of attack. Circumferential pressure distributions (referred to the local pressure on the stagnation line) were relatively insensitive to location along cone generators even at large angles of attack. L 1 6 2 4

Heat-transfer distributions were predicted satisfactorily up to 60° away from the windward generator by Lees' heat-transfer distribution based on circumferential Newtonian pressures. Beyond 60° experimental values of heat transfer were somewhat higher than the theoretical prediction but these areas are of secondary importance because of their low heating rates.

Effects of Bluntness

Measurements on the blunt cone were made beyond two nose radii from the point of tangency. In general, for this area, results for the blunt cone differed from those of the sharp cone by an amount less than the experimental scatter. At angles of attack of 0° and 90° some differences with the sharp cone were found. At an angle of attack of 0° blunt-cone data within eight nose radii from the point of tangency showed lower pressures and heat-transfer coefficients (based on normal-shock entropy) than the corresponding points on the sharp cone.

Langley Research Center,
National Aeronautics and Space Administration,
Langley Air Force Base, Va., July 27, 1961.

REFERENCES

1. Van Driest, E. R.: Turbulent Boundary Layer on a Cone in a Supersonic Flow at Zero Angle of Attack. Jour. Aero. Sci., vol. 19, no. 1, Jan. 1952, pp. 55-57, 72.

2. Braun, Willis H.: Turbulent Boundary Layer on a Yawed Cone in a Supersonic Stream. NASA TR R-7, 1959. (Supersedes NACA TN 4208.)

3. Dorrance, William H., and Romig, Mary F.: The Effect of Blunting a Cone on Conical Surface Reynolds Number and Laminar Flow Heat Transfer at Hypersonic Mach Numbers. Rep. No. ZA-7-015, Convair, Mar. 11, 1955.

4. Julius, Jerome D.: Measurements of Pressure and Local Heat Transfer on a 20° Cone at Angles of Attack up to 20° for a Mach Number of 4.95. NASA TN D-179, 1959.

5. Jones, Robert A., and Gallagher, James J.: Heat-Transfer and Pressure Distributions of a 60° Swept Delta Wing With Dihedral at a Mach Number of 6 and Angles of Attack From 0° to 52°. NASA TM X-544, 1961.

6. Conti, Raul J.: Approximate Temperature Distributions and Streamwise Heat Conduction Effects in the Transient Aerodynamic Heating of Thin-Skinned Bodies. NASA TN D-895, 1961.

7. Beckwith, Ivan E.: Similar Solutions for the Compressible Boundary Layer on a Yawed Cylinder With Transpiration Cooling. NASA TR R-42, 1959. (Supersedes NACA TN 4345.)

8. Lees, Lester: Laminar Heat Transfer Over Blunt-Nosed Bodies at Hypersonic Flight Speeds. Jet Propulsion, vol. 26, no. 4, Apr. 1956, pp. 259-269, 274.

9. Van Driest, E. R.: Investigation of Laminar Boundary Layer in Compressible Fluids Using the Crocco Method. NACA TN 2597, 1952.

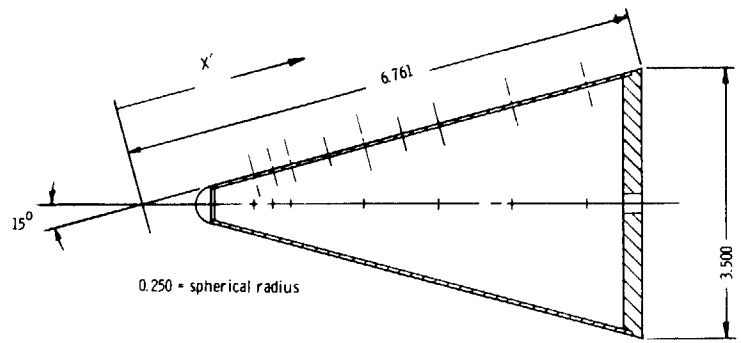

Thermocouple locations:

X' = 1.50; 1.75; 2.00; 2.50; 3.00; 3.50; 4.00; 5.00; 6.00

Pressure-tube locations:

X' = 1.50; 1.75; 2.00; 3.00; 4.00; 5.00; 6.00

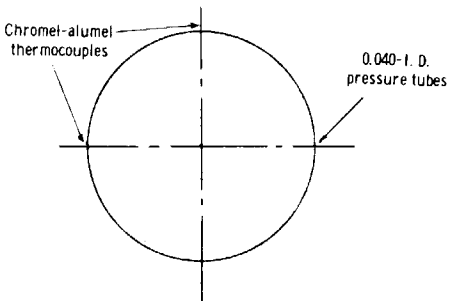

t = 0.030 ± 0.001

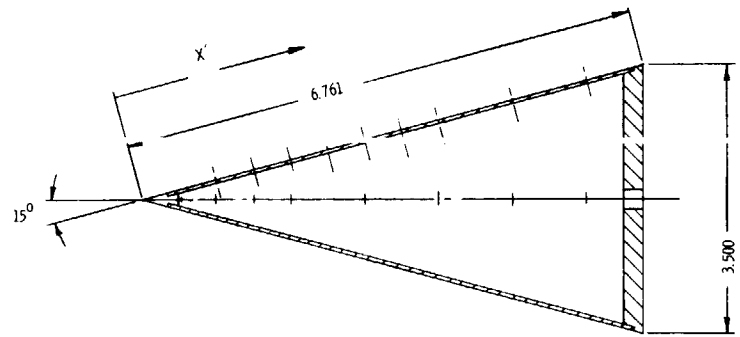

Thermocouple locations:

X' = 1.00; 1.50; 2.00; 2.50; 3.00; 3.50; 4.00; 5.00; 6.00

Pressure-tube locations:

X' = 0.50; 1.00; 1.50; 2.00; 3.00; 4.00; 5.00; 6.00

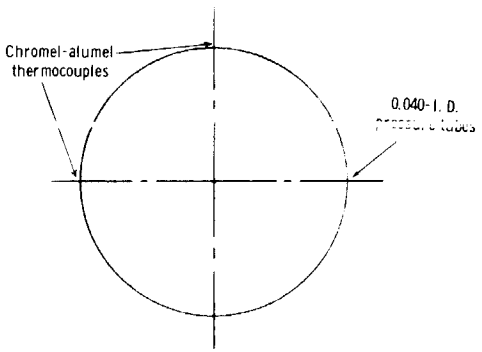

X'	t
1	0.037
1.5	.034
2.0	.028
2.5	.028
3.0	.028
3.5	.029
4.0	.030
5.0	.030
6.0	.031

Figure 1.- Cone models. All dimensions are in inches. Material is 347 stainless steel.

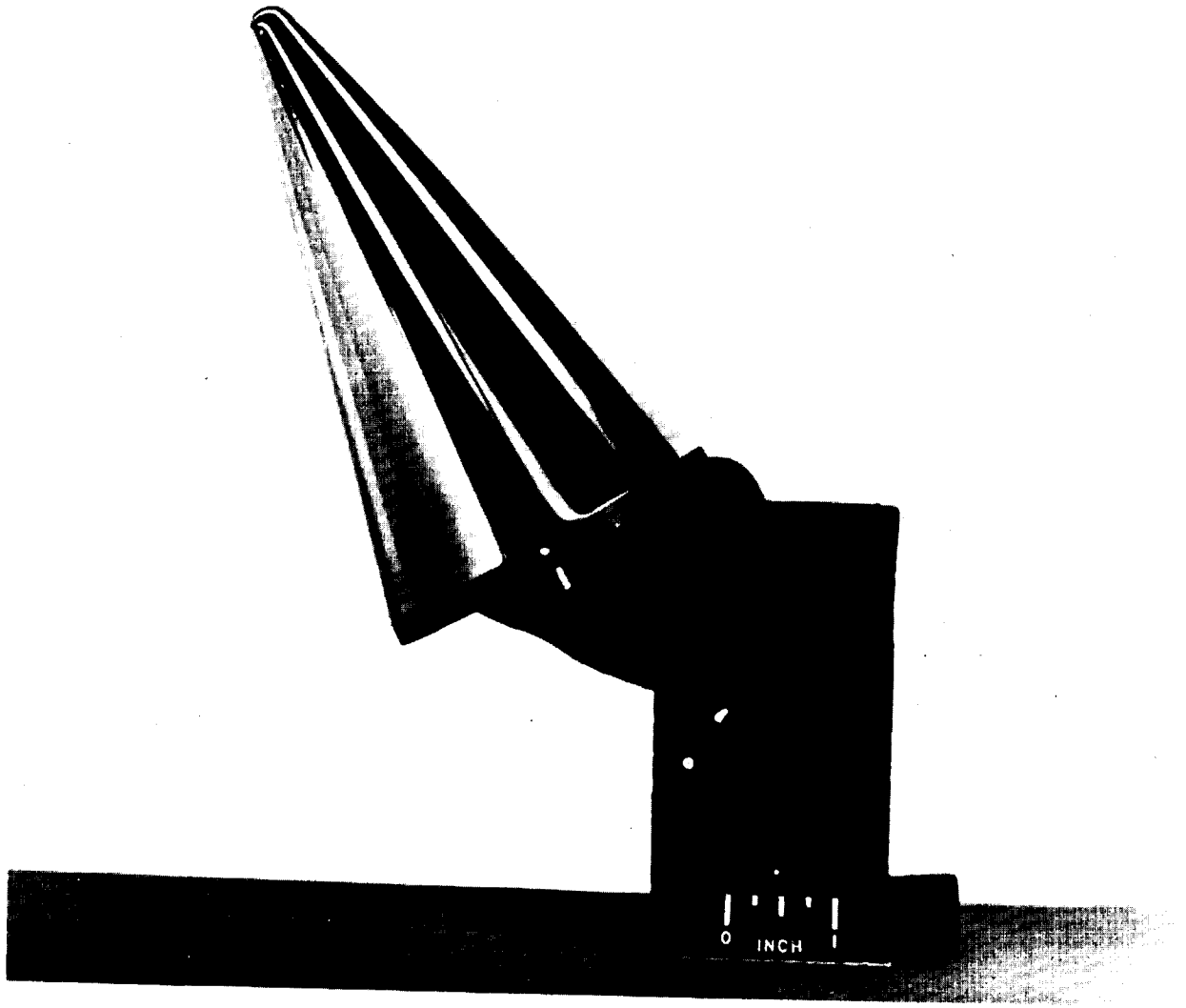

Figure 2.- Blunt cone mounted on strut. L-61-1401

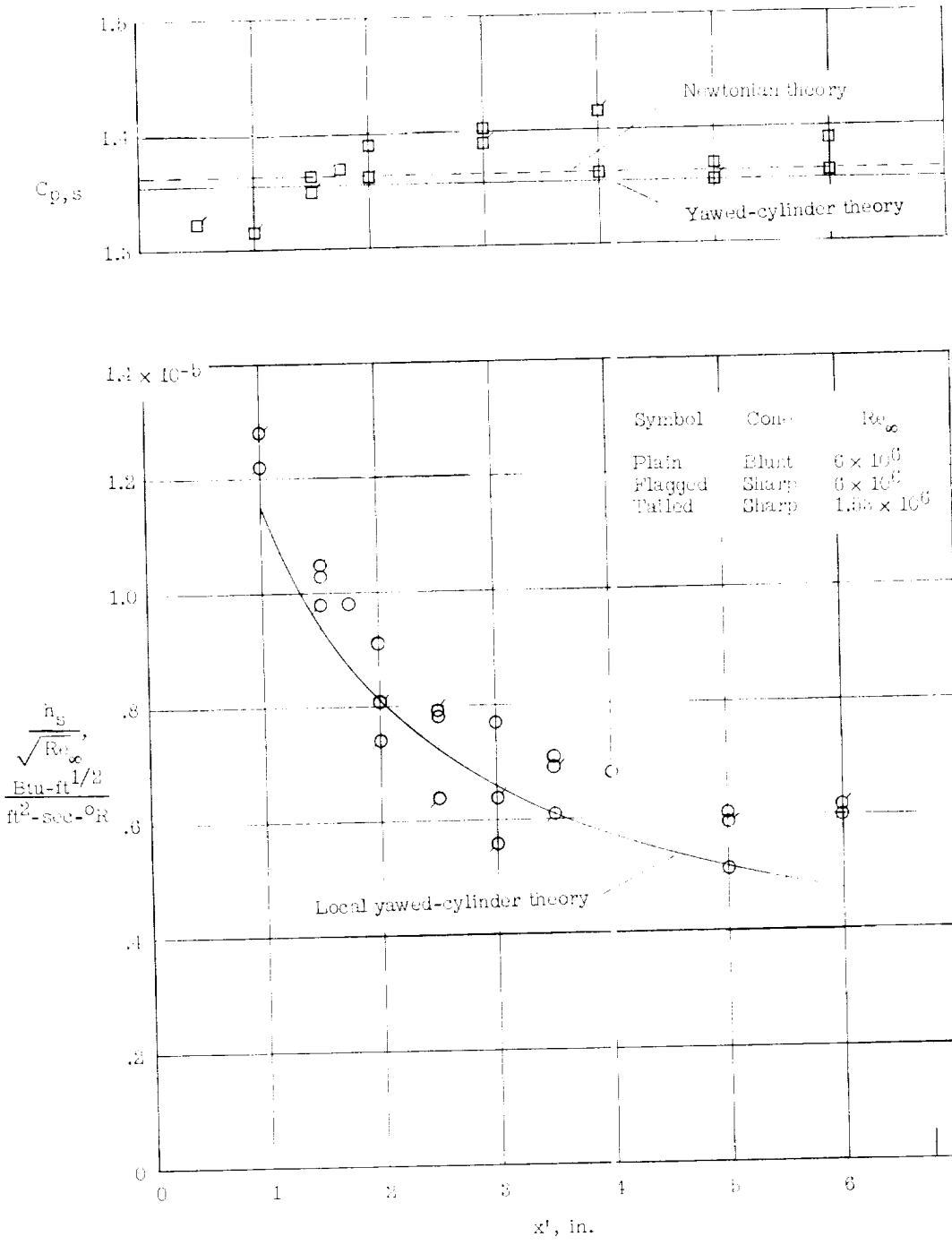

(a) $\alpha = 45^\circ$.

Figure 3.- Heat-transfer and pressure distributions on stagnation line.

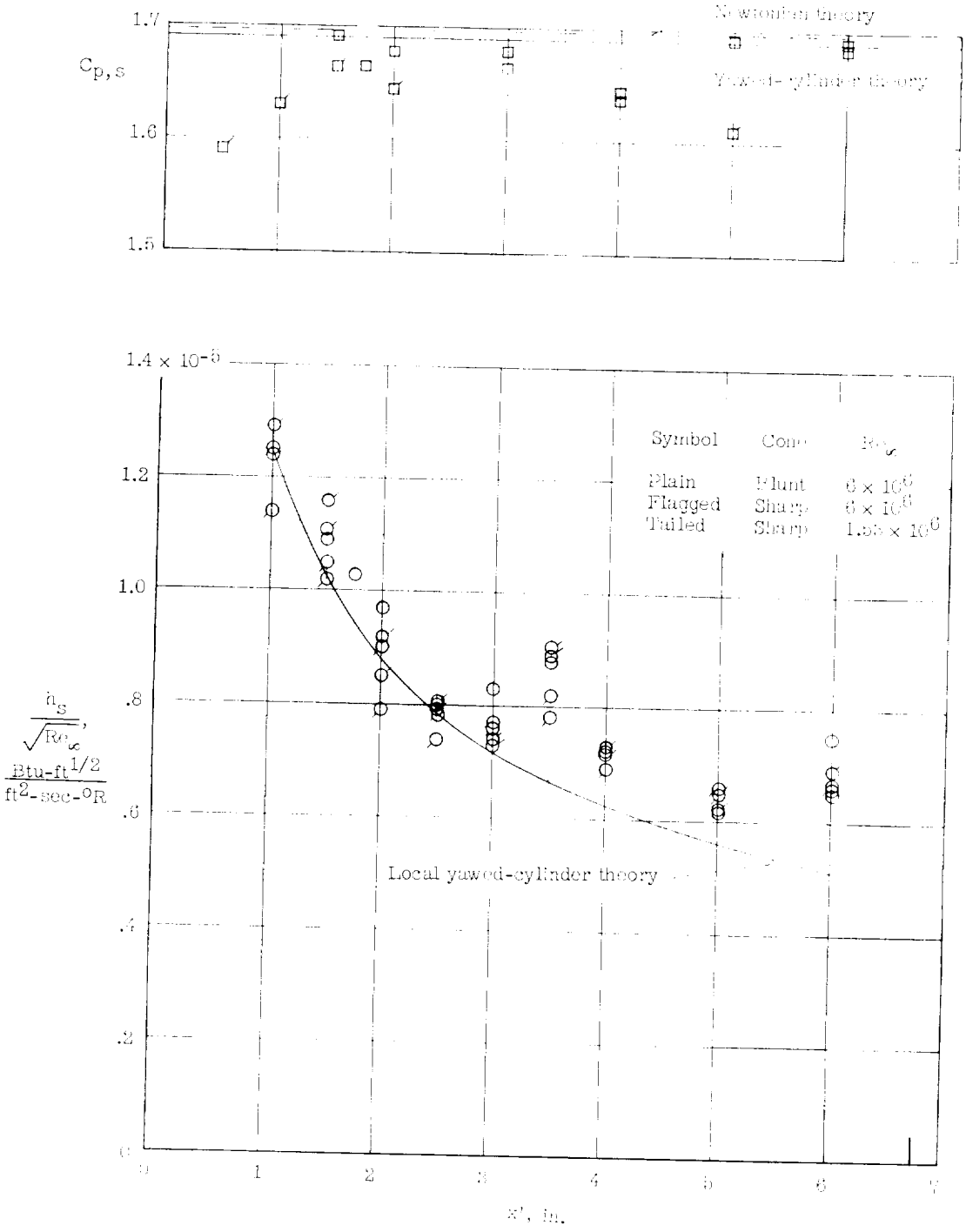

(b) $\alpha = 60^\circ$.

Figure 3.- Continued.

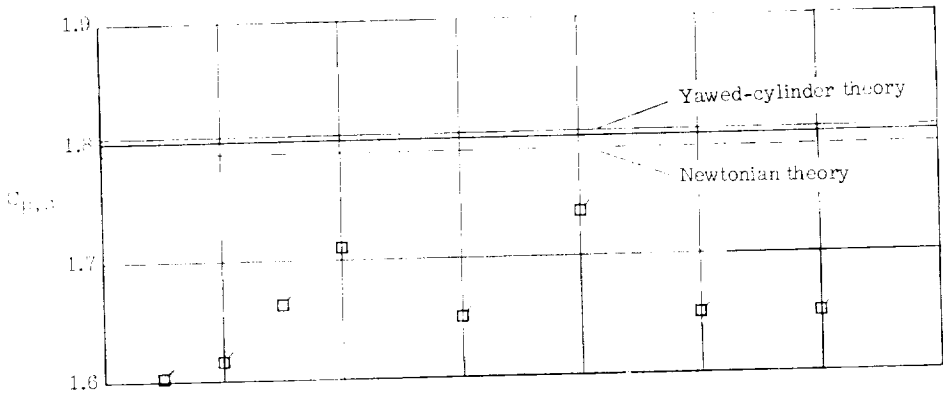

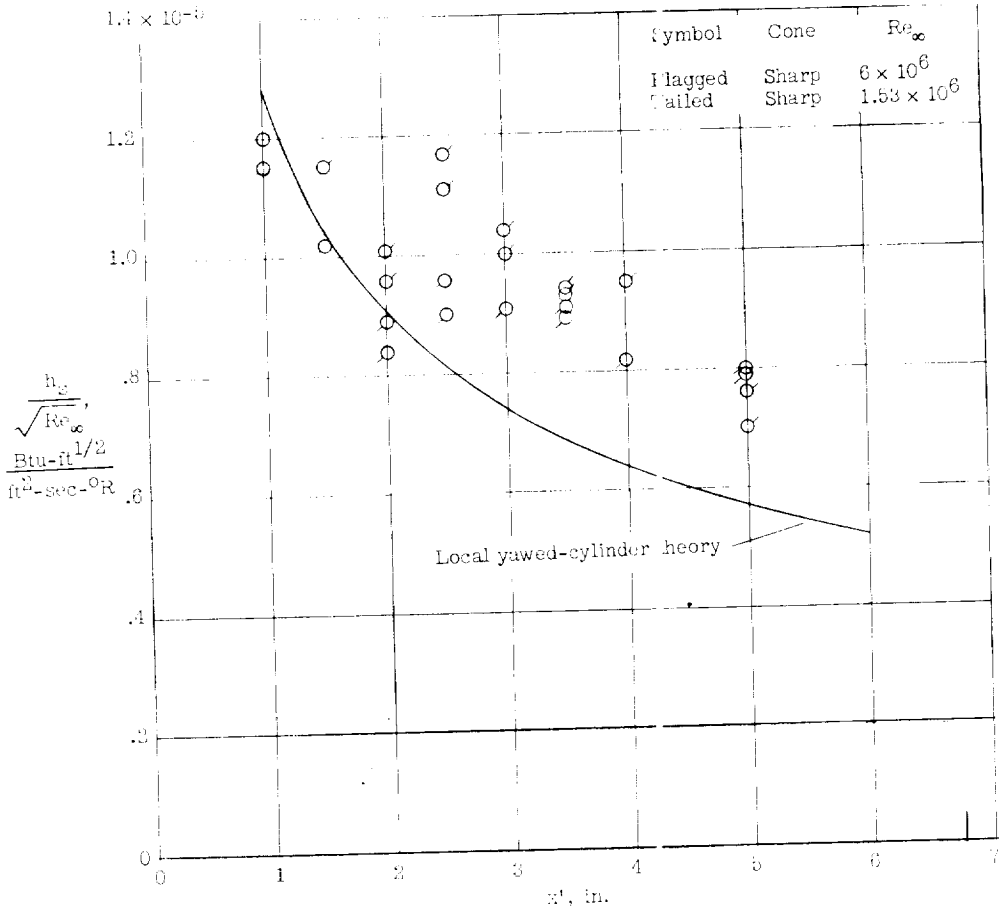

(c) $\alpha = 70^o$.

Figure 3.- Continued.

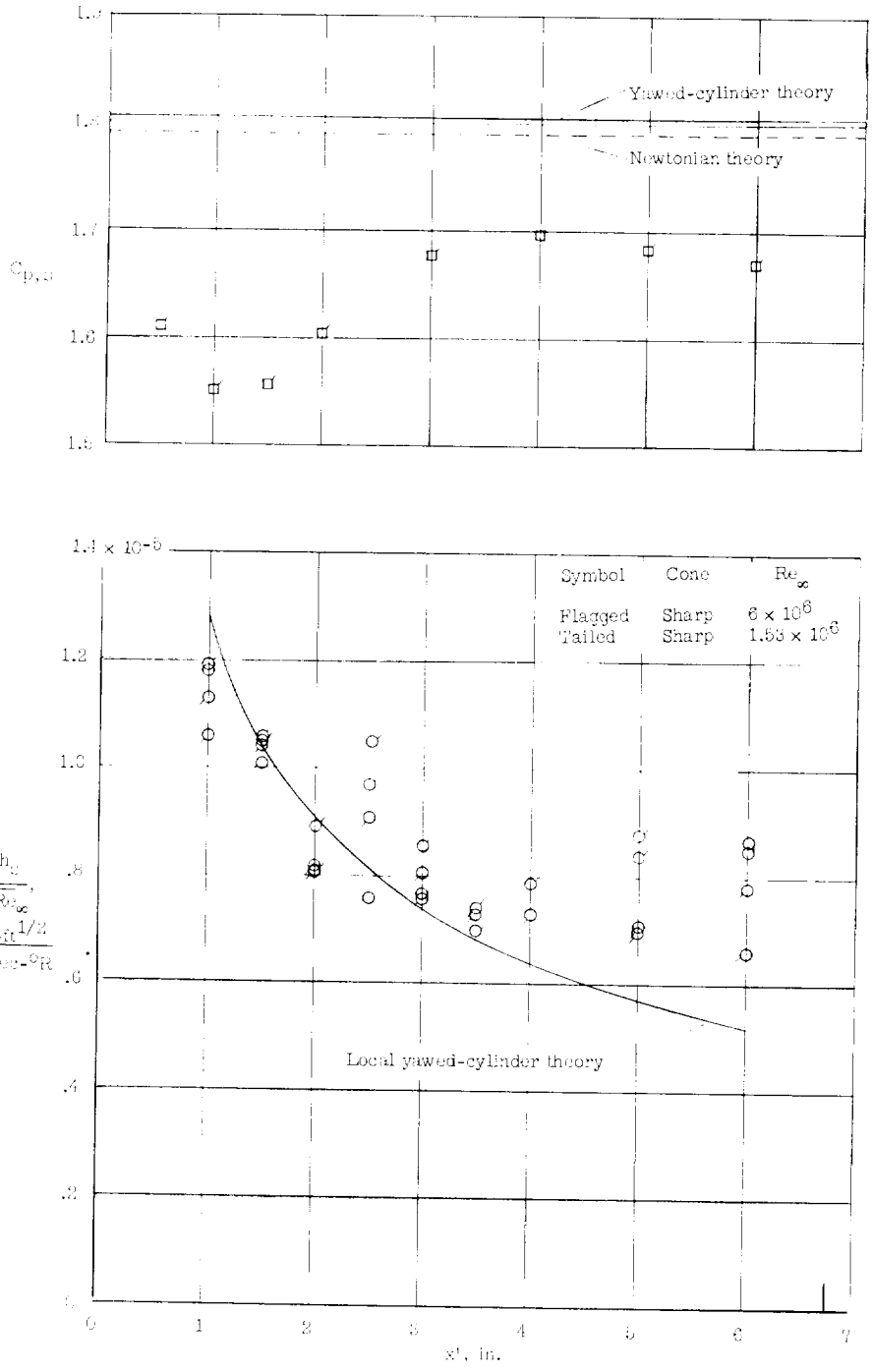

(d) $\alpha = 80^\circ$.

Figure 3.- Continued.

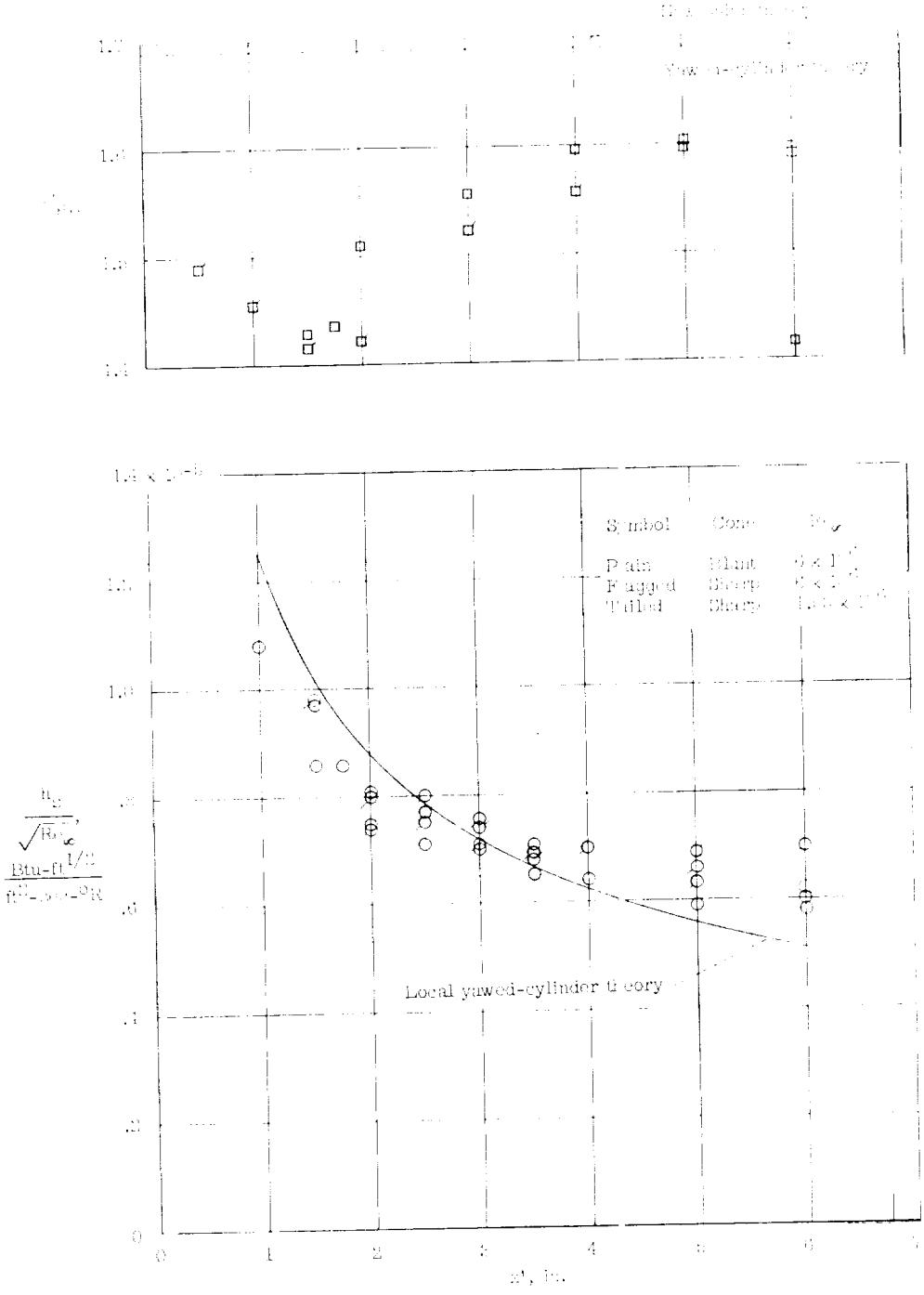

(e) $\alpha = 90^{\circ}$.

Figure 3.- Concluded.

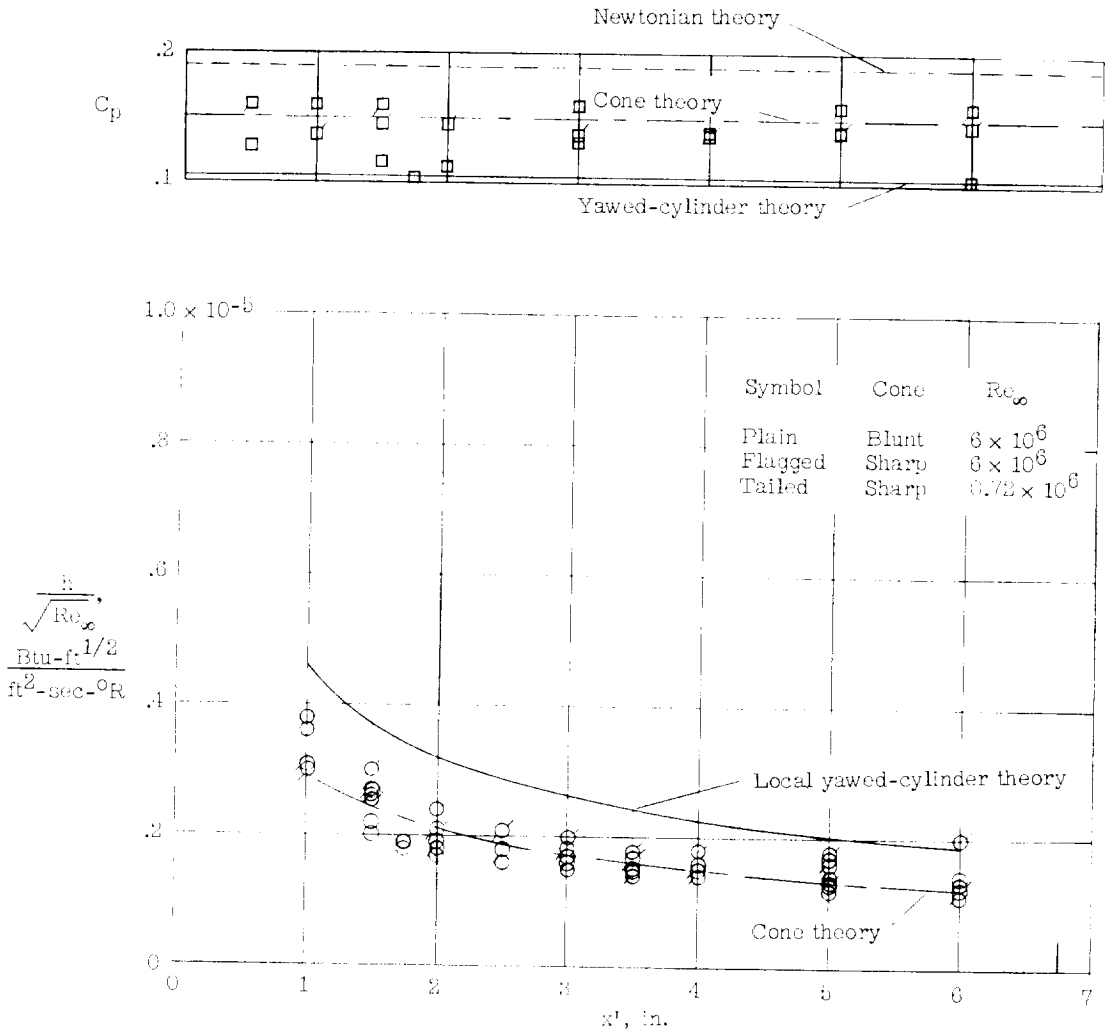

Figure 4.- Heat-transfer and pressure distributions at an angle of attack of 0^o.

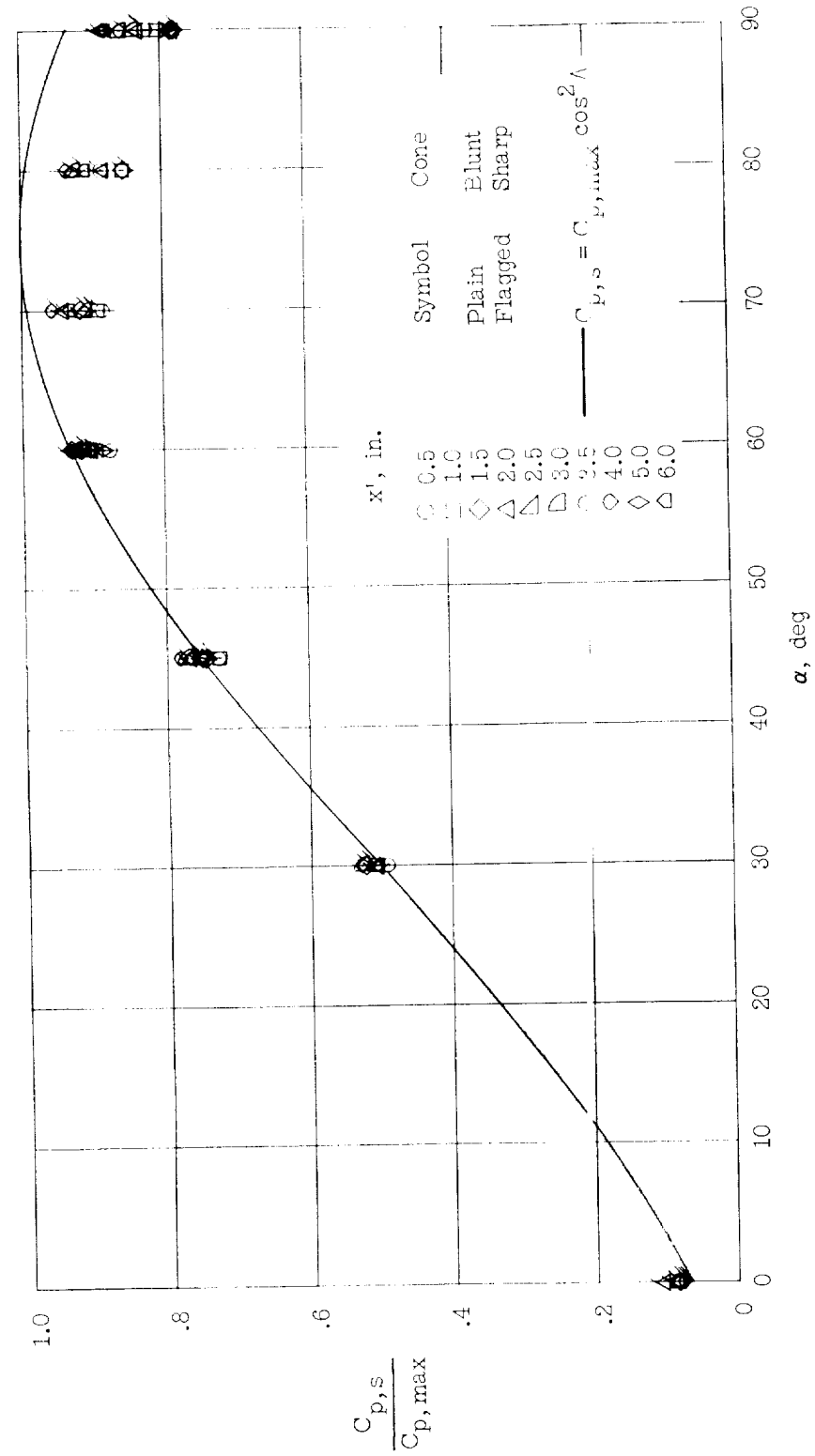

Figure 5.- Pressure coefficient on stagnation line. $Re_\infty = 6 \times 10^6$.

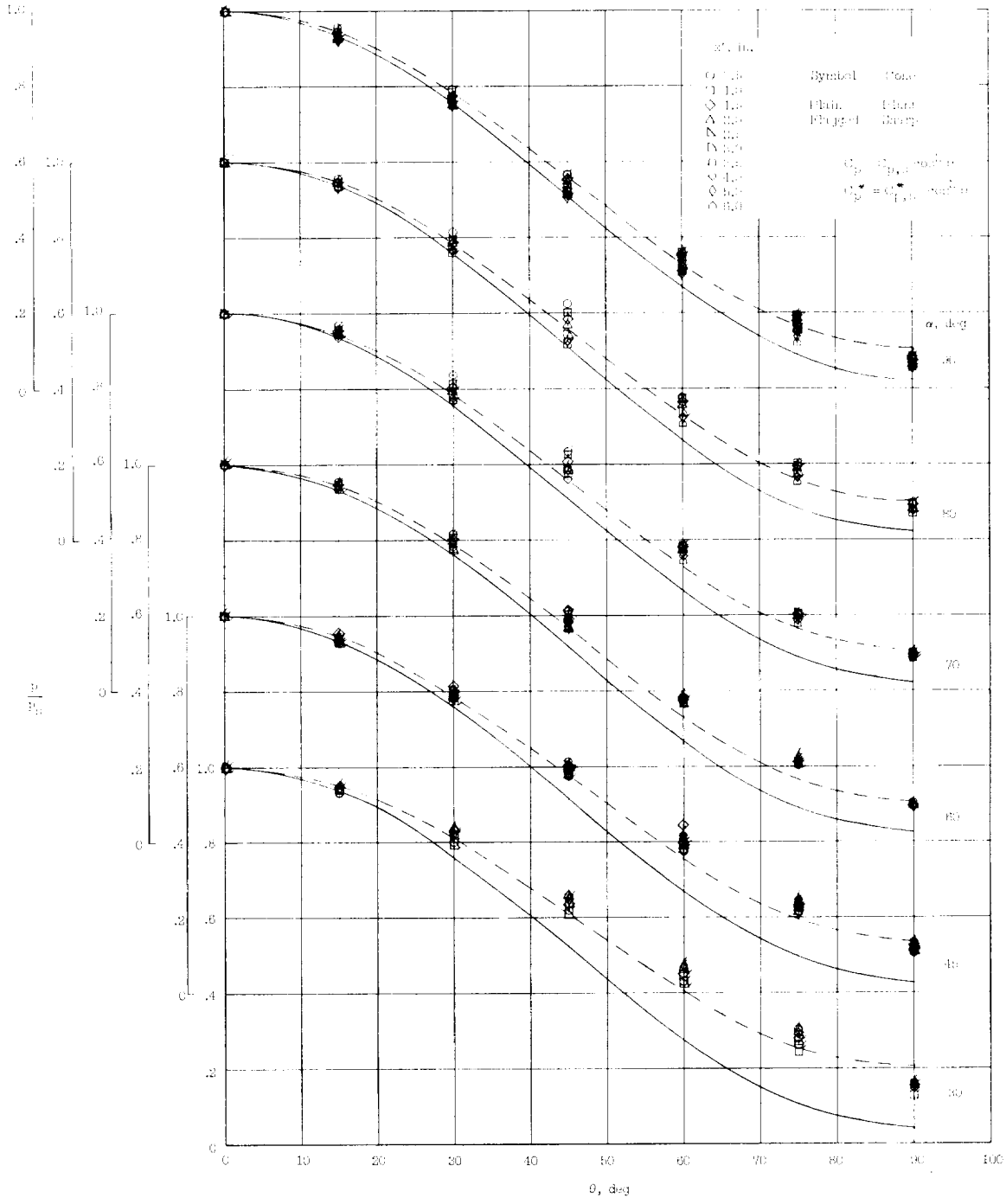

Figure 6.- Circumferential pressure distributions at various angles of attack. $Re_\infty = 6 \times 10^6$.

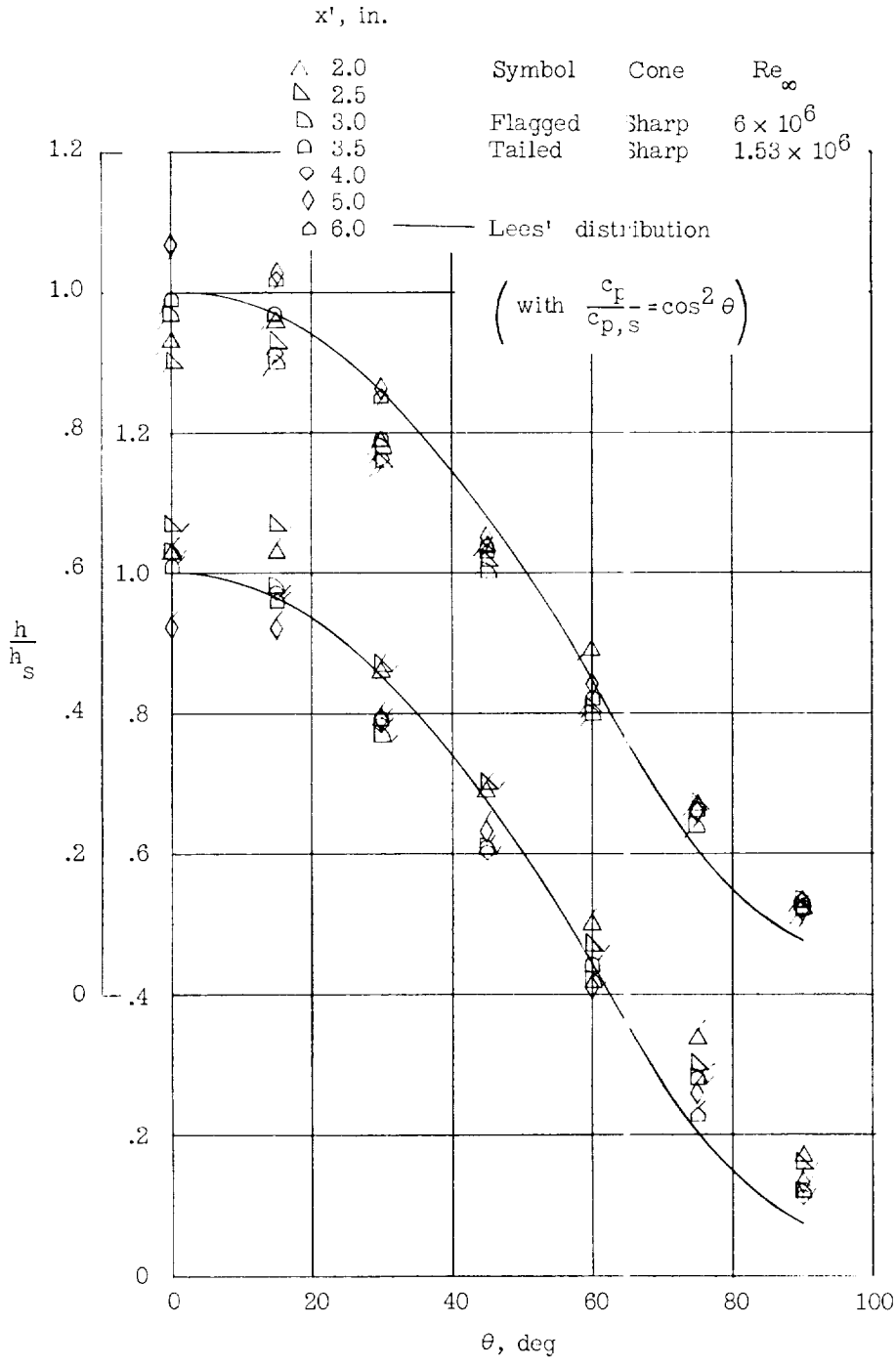

(c) $\alpha = 70^\circ$.

Figure 7.- Continued.

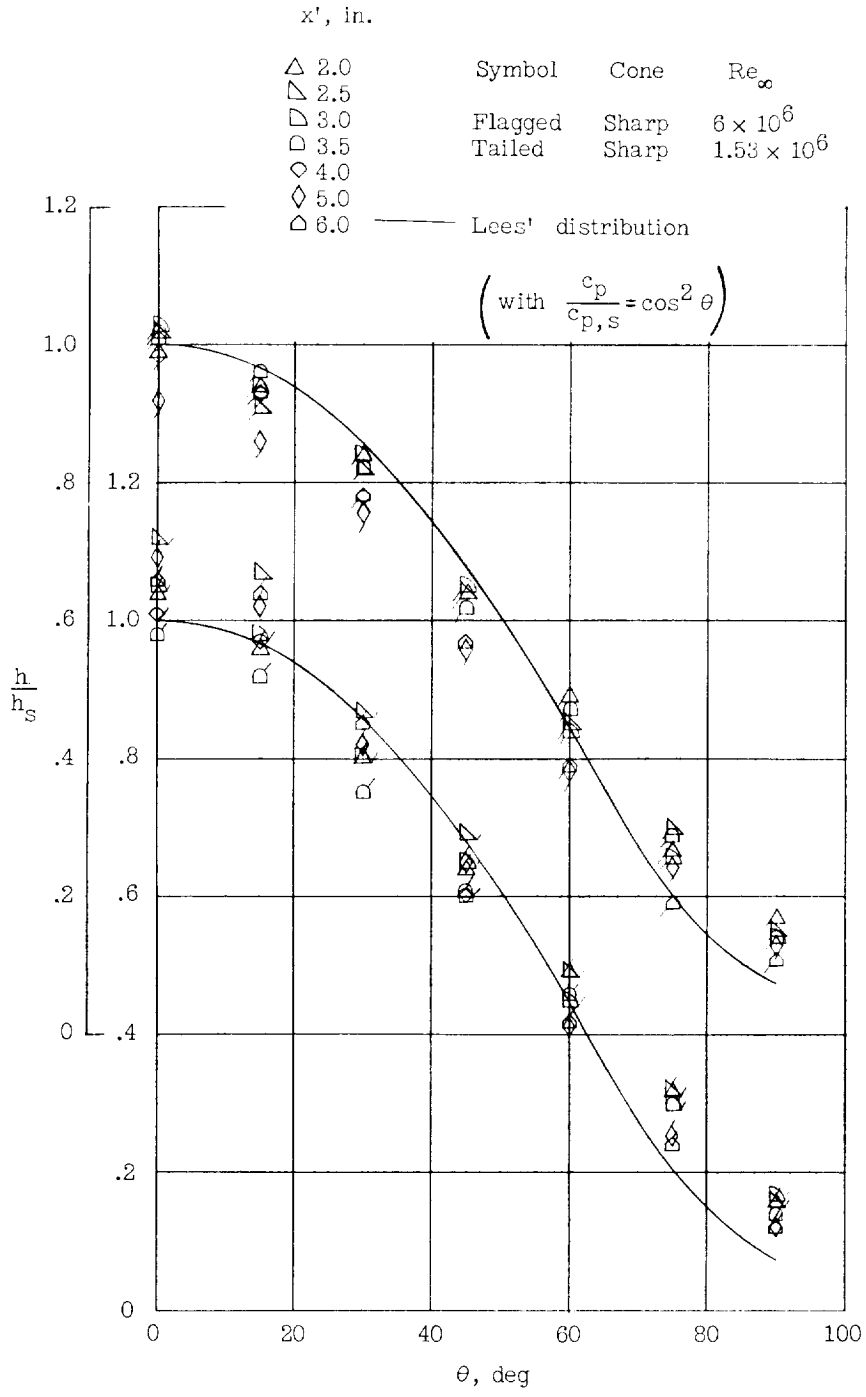

(d) $\alpha = 80^\circ$.

Figure 7.- Continued.

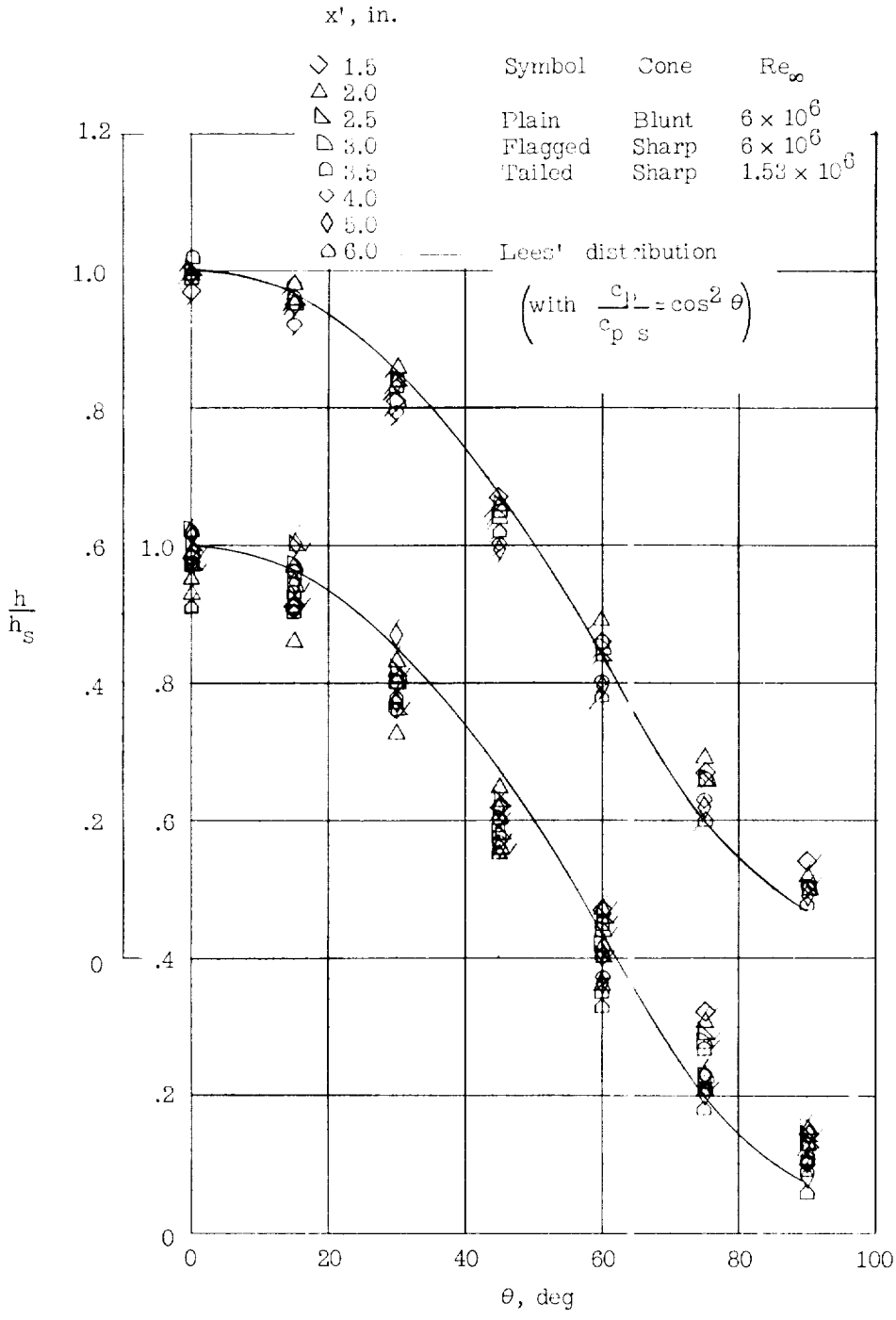

(e) $\alpha = 90^\circ$.

Figure 7.- Concluded.

(a) Sharp cone at $\alpha = 0^\circ$.

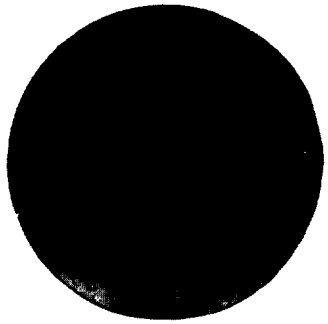

(b) Blunt cone at $\alpha = 0^\circ$.

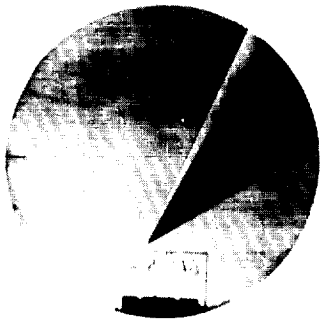

(c) Sharp cone at $\alpha = 45^\circ$.

(d) Blunt cone at $\alpha = 45^\circ$.

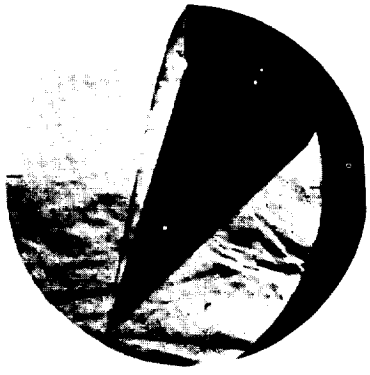

(e) Sharp cone at $\alpha = 60^\circ$.

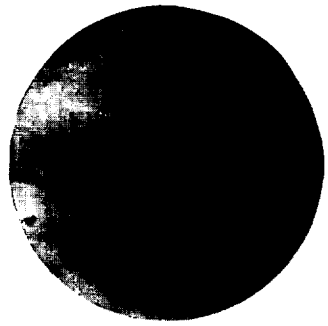

(f) Blunt cone at $\alpha = 60^\circ$.

L-61-5067

Figure 8.- Schlieren pictures of the flow about the models. Tick marks at edges of window denote ends of wire locating tunnel center line.

(g) Sharp cone at $\alpha = 70^{\circ}$.

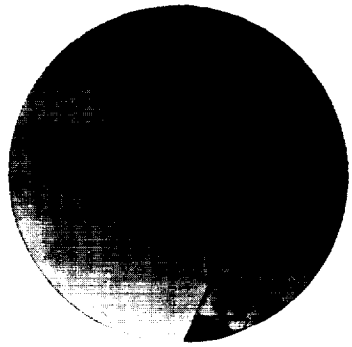

(h) Sharp cone at $\alpha = 80^{\circ}$.

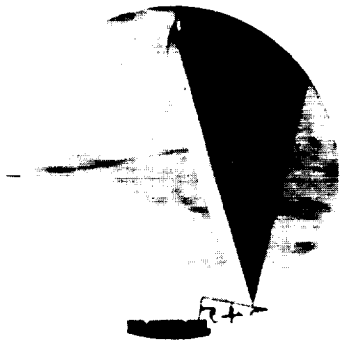

(i) Sharp cone at $\alpha = 90^{\circ}$.

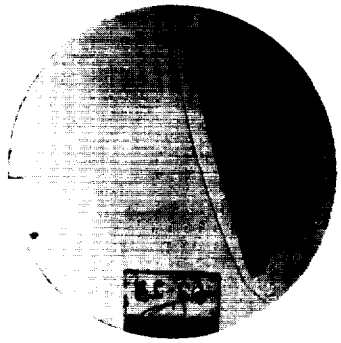

(j) Blunt cone at $\alpha = 90^{\circ}$.

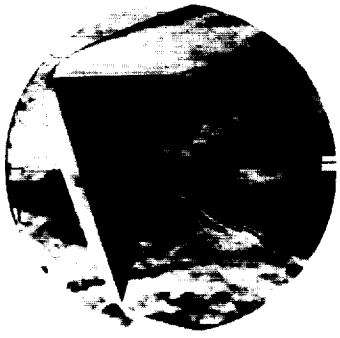

(k) Full-scale version of sharp cone at $\alpha = 90^{\circ}$.

(l) 0.68-scale version of sharp cone at $\alpha = 90^{\circ}$.

Figure 8.- Concluded. L-61-5068

NASA-Langley, 1961 L-1624

L-1624